RASĀYAN *J. Chem.*
Vol. 19 | No. 2 | 831-838| April-June | 2026
ISSN: 0974-1496 | e-ISSN: 0976-0083 | CODEN: RJCABP
http://www.rasayanjournal.com
http://www.rasayanjournal.co.in

SYNTHESIS, CHARACTERIZATION AND EMISSION STUDIES OF Eu^{3+}/ Dy^{3+} DOPED $K_2Mo_4O_{13}$ PHOSPHORS

S. Dhilleswararao[1,2] and S. Ramakrishna[1,3,✉]

[1]Research Centre, Government Degree College for Men, Srikakulam, Andhra Pradesh, affiliated to Dr. B. R. Ambedkar University, Etcherla-532410, (Andhra Pradesh) India

[2]Department of Chemistry, Government Degree College, Tuni-533401, (Andhra Pradesh) India

[3]Department of Chemistry, Government Degree College for Men, Srikakulam-532001, (Andhra Pradesh) India

✉Corresponding author: s7ramakrishna@gmail.com

ABSTRACT

Alkali molybdates are of considerable interest due to their remarkable properties and possible applications. Potassium tetra molybdate ($K_2Mo_4O_{13}$) was prepared by the standard solid-state method, while the rare earth (Eu^{3+} and Dy^{3+}) doped $K_2Mo_4O_{13}$ compositions were obtained from a simple ion exchange method. The materials were characterised by powder X-ray diffraction (XRD), Scanning electron microscope-Energy dispersive spectroscopy (SEM-EDS), Fourier transform Infra-red spectroscopy (FT-IR) and Raman techniques. Parent $K_2Mo_4O_{13}$, and Eu^{3+} / Dy^{3+} doped $K_2Mo_4O_{13}$ compositions formed a triclinic phase. The Infra-red and Raman spectra gave bands in the 400-1000 cm^{-1}, consistent with reported spectra. The SEM images consist of rod-like structures in both parent and Ln-doped KMO. The EDS profiles of Ln (Ln = Eu and Dy) doped KMO consist of peaks corresponding to Ln, K, Mo and O. The photoluminescence (PL) excitation spectra are dominated by 4f-4f transitions. The PL excitation spectra of Eu (Dy) consist of an intense peak at 395 nm (427 nm) and are related to the $^7F_0 \rightarrow {}^5L_6$ ($^6H_{15/2} \rightarrow {}^4G_{11/2}$) transition of the Ln ion and a few low-intense lines. The emission spectra of Eu (Dy) have a strong band at 615 nm (638 nm) and are related to the transitions of $^5D_0 \rightarrow {}^7F_2$ ($^4F_{9/2} \rightarrow {}^6H_{11/2}$). The Eu (Dy) doped KMO phosphor materials emitted the red (deep red) colour light, which may be useful for the preparation of the W-LEDs.

Keywords: Potassium Tetramolybdate, Phosphors, Photoluminescence, Solid-State Synthesis, Rare-Earth Doping, W-LEDs.

RASĀYAN *J. Chem.*, Vol. 19, No.2, 2026

INTRODUCTION

Incandescent bulbs and flashlights have been replaced (or in the process of being replaced) by white light-emitting diodes (W-LEDs) owing to their remarkable characteristics such as high luminous efficiency, energy saving (low energy consumption), high reliability, high durability, small volume, long operation lifetime and environmental friendliness.[1,2] The W-LEDs are fabricated by coating appropriate amounts of yellow phosphor (YAG: Ce^{3+}) over a blue-emitting GaN or InGaN chips.[2] Nevertheless, this W-LED (YAG: Ce^{3+} and GaN/InGaN) has certain demerits like poor colour rendering index (CRI), absence of red component leading to narrow visible range, and thermal quenching at high temperatures.[3,4] These demerits prevent such W-LEDs from penetrating the general lighting market. Efforts were made to improve the CRI by introducing red-emitting phosphors such as Na_2SiF_6:Mn^{4+}, CdSe-Sr_3SiO_5:Ce^{3+}, Li^+, and $Sr_2Si_5N_8$:Eu^{2+}.[5,6,7] Unfortunately, these red-emitting phosphors also possess certain undesirable properties such as unacceptable toxicity levels, meagre chemical stability, corrosive precursors, difficult preparation procedure, or high cost. Thus, the search for new red-emitting phosphors with desirable characteristics is worthy of investigation and challenging. Molybdenum-based oxides have interesting properties such as high ionic conductivity, good catalytic activity, and good lasing efficiency.[8-10] Further, molybdates containing rare earth ions have impending applications due to their luminescent, piezoelectric, ferro elastic, ferroelectric and laser properties.[11] In recent years, several investigations on the luminescence behaviour of rare-earth-doped molybdates have been reported. Molybdenum with variable valency and coordination number forms different structural motifs, which are partly responsible for these properties. One such structural arrangement is a layer (ribbon) type lattice adopted by $K_2Mo_4O_{13}$ with K^+ ions

http://doi.org/10.31788/RJC.2026.1929609

residing between the broken ribbons of the MO_n polyhedra.[12] These potassium ions are replaceable with the same or different valency ions even at room temperature. This property was exploited to prepare rare-earth-doped $K_2Mo_4O_{13}$ compositions by stirring solid $K_2Mo_4O_{13}$ in aqueous $LnCl_3$ solution at ambient temperature. In the present investigation, the emission results of Eu^{3+} and Dy^{3+} $K_2Mo_4O_{13}$ are presented.

EXPERIMENTAL

Materials and Chemicals

All the chemicals involved in the preparation of $K_2Mo_4O_{13}$, Eu-doped $K_2Mo_4O_{13}$, and Dy-doped $K_2Mo_4O_{13}$ were analytical grade (AR), and these were used without any further purification. Potassium nitrate (KNO_3, ≥ 99% purity), molybdenum trioxide (MoO_3, ≥ 99% purity), europium (III) chloride anhydrous ($EuCl_3$, 99.99% trace metals basis), dysprosium (III) chloride anhydrous ($DyCl_3$, 99.99% trace metals basis) and acetone (CH_3COCH_3, ≥ 99% purity) were all procured from Sigma-Aldrich, Bengaluru, India and were used as received.

General Procedure

The polycrystalline $K_2Mo_4O_{13}$ was prepared by using the well-known solid-state reaction method, as reported by Gatehouse *et al*., except for the source of K^+.[12] The reactants KNO_3 and MoO_3 were taken in a 2:4 molar ratio for a final product weight of 5 g and thoroughly ground in an agate mortar in the presence of acetone, which assists in the formation of a homogeneous mixture and evaporates during the grinding process. The resultant powder was loaded into a porcelain crucible and heated at 400^0C for 10 h and 600^0C for 48 h with two intermittent grindings. A colourless product was obtained. The Eu^{3+} and Dy^{3+} ions were doped into the host $K_2Mo_4O_{13}$ lattice through a facile ion exchange method at room temperature. In this method, the stoichiometric ratio of the solid $K_2Mo_4O_{13}$ and $EuCl_3$ ($DyCl_3$) solution is used. Required volume of 0.05 M $EuCl_3$ ($DyCl_3$) solution was vigorously stirred with solid $K_2Mo_4O_{13}$ for 24 hours. A total of five Eu-doped $K_2Mo_4O_{13}$ (0.06, 0.08, 0.1, 0.12 and 0.14 mol% of Eu) and four Dy-doped $K_2Mo_4O_{13}$ (0.04, 0.06, 0.08 and 0.1 mol% of Dy) were prepared. The supernatant solution was carefully separated from the solid (product-1). The Eu and DY doped $K_2Mo_4O_{13}$ are designated as KMO-Eu and KMO-Dy, respectively. The supernatant solution was carefully heated to dryness. The obtained solid is named "product-2". Both product-1 and product-2 are subjected to powder XRD.

Detection Method

A Rigaku MiniFlex 600 X-ray diffractometer with Cu K_α radiation (λ = 1.5406 Å) was used to record the XRD profiles of prepared materials. The 2θ range was 5-80 with a step width of 0.020 and a step time of 0.15s. The Zeiss EVO 18 model scanning electron microscope with energy dispersive spectroscopy was used to study the surface morphology of as-prepared materials. FT-IR spectra were obtained over the range of 400-4000 cm^{-1} using a Shimadzu 8400 spectrometer. The Raman measurements were performed on powdered samples with a Horiba Hr 800 employing a 532 nm He–Ne laser. The Shimadzu RF-6000-spectrofluorophotometer was employed to obtain photoluminescence emission as well as excitation spectral measurements of Eu (Dy) activated samples.

RESULTS AND DISCUSSION

X-Ray Powder Diffraction

The X-ray powder diffraction patterns of KMO ($K_2Mo_4O_{13}$), product-1 (Eu-doped $K_2Mo_4O_{13}$ (KMO-Eu) and Dy-doped $K_2Mo_4O_{13}$ (KMO-Dy)) and product-2 are shown in the Fig.-1. All the patterns of KMO and product-1 (KMO-Eu and KMO-Dy) are free from impurities with negligible background, indicating the crystalline nature of the samples. All the *d*-lines of KMO are similar to the reported ICDD card number 27-0416.[12] It is reported that KMO crystallises in a triclinic lattice with a = 7.97, b = 8.34, c = 10.01 Å; α = 107.1, β = 102.88, γ = 109.76^0 with Z = 2 and $P\bar{1}$ space group.[12] The structure of KMO is characterised by infinite broken ribbons consisting of four MoO_6 edge-shared octahedral units running along the [010] plane. These four octahedral units are then linked to identical four MoO_6 units by edge sharing. These eight units link to another eight units and form infinite chains along the *b*-axis. No common oxygen atoms are present between adjacent chains. Potassium ions are located between the broken ribbons and can be replaced with guest ions.[12,13] The powder patterns of KMO-Eu and KMO-Dy are also similar and

consistent with JCPDF No: 27-0416. The powder pattern is expanded in the 22.5-30^0 region and shown in Fig.-1. A shift of d-lines towards higher 2θ values authenticates the substitutions of Eu^{3+} and Dy^{3+} ions into the KMO lattice. The shift in the 2θ can be attributed to the difference in the ionic size of K^+ (1.51 Å for 8 coordination), Eu^{3+} (1.07 Å for 9 coordination) and Dy^{3+} (1.03 Å for 9 coordination). The similarity of XRD patterns of KMO-Eu and KMO-Dy with parent KMO suggests that these doped compositions also crystallised in a triclinic lattice. The powder pattern of the product-2, obtained by heating the supernatant solution, gave *d*-lines at 2θ = 24.6, 28.5, 40.7, 48.1, 50.4, 58.98, and 74 (Fig.-1c). These *d*-lines correspond to the KCl lattice with ICDD No.89-3619. Thus, the reaction can be written as.

$$K_2Mo_4O_{13}\ (solid) + LnCl_3(aqueous) \xrightarrow{stirring} K_{2-3x}Ln_xMo_4O_{13}\ (solid) + x\ KCl\ (solution)$$
$$(Ln = Eu, Dy) \qquad (product\ 1)$$

$$KCl\ (solution) \xrightarrow{heat} KCl\ (solid)$$
$$(product\ 2)$$

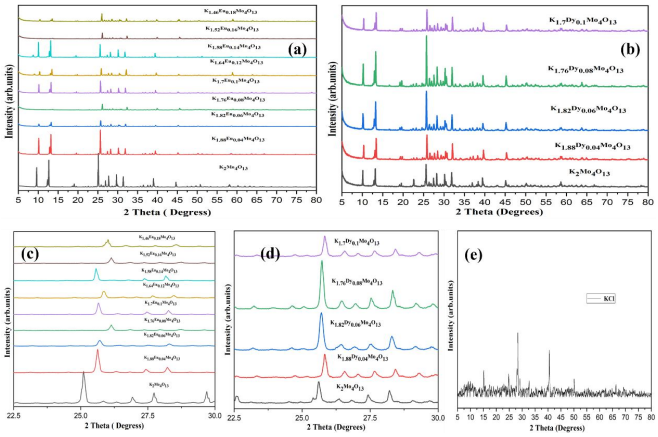

Fig.-1: Powder XRD Patterns of (a) KMO-Eu and (b) KMO-Dy. Peak Shift in 2θ of (c) KMO-Eu and (d) KMO-Dy the Powder Pattern of (e) Product 2 (KCl)

Scanning Electron Microscopy

The morphology of KMO and KMO-Eu (KMO-Dy) was studied by recording the FESEM images of representative compositions and depicted in Fig.-2. The images exhibit rod-like objects for both KMO and KMO-Eu (KMO-Dy) with substantial agglomeration. The EDS profile of KMO exhibits peaks corresponding to elements K, Mo and O. The EDS of KMO-Eu (KMO-Dy) shows peaks corresponding to Eu (Dy) in addition to peaks of K, Mo and O (Fig.-3). The EDS results support the doping of Eu (Dy) into the KMO lattice. The elemental mapping also supports the incorporation of Eu (Dy) into the KMO lattice, as shown in Fig.-4.

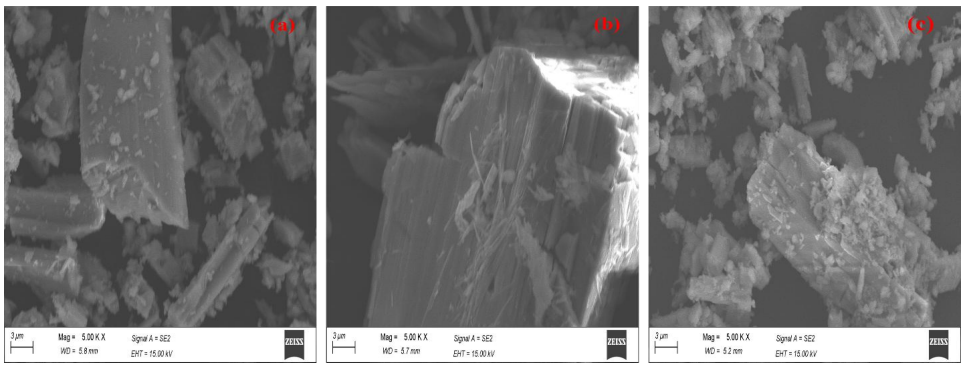

Fig.-2: SEM Images of (a) KMO, (b) $K_{1.76}Eu_{0.08}Mo_4O_{13}$, and (c) $K_{1.76}Dy_{0.08}Mo_4O_{13}$

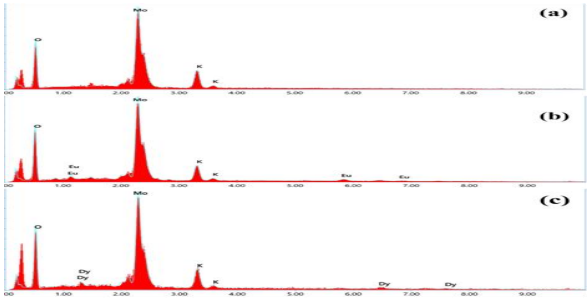

Fig.-3: EDS Profiles of (a) KMO, (b) $K_{1.76}Eu_{0.08}Mo_4O_{13}$, and (c) $K_{1.76}Dy_{0.08}Mo_4O_{13}$

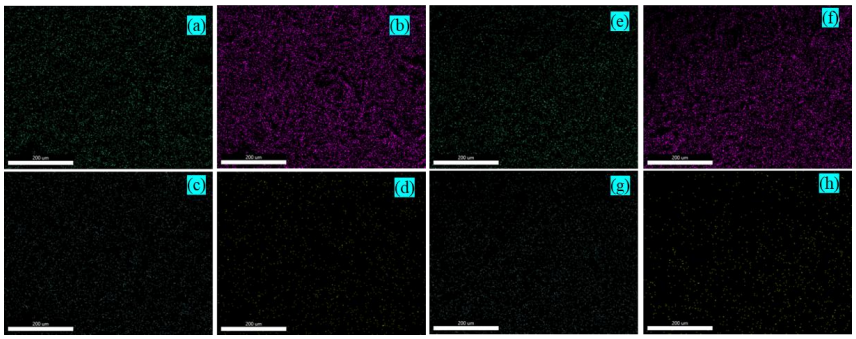

Fig.-4: Elemental Mapping of $K_{1.76}Eu_{0.08}Mo_4O_{13}$ (a) K (b) Mo (c) O and (d) Eu, and Elemental Mapping of $K_{1.76}Dy_{0.08}Mo_4O_{13}$ (e) K (f) Mo (g) O and (h) Dy

Fourier Transform Infra-Red Spectroscopy

The phase formation of KMO was further supported by recording the FT-IR spectra in the 400-4000 cm^{-1} range. The FT-IR spectra of parent KMO and representative Eu (Dy) doped KMO are provided in the Fig.-5A, in the range 400-1000 cm^{-1}. No prominent bands were observed in the 1000-4000 cm^{-1} range. These spectra are similar to each other and comparable with reported spectra.[14,15] The spectra are characterised by the strong bands in the 400-900 cm^{-1} and are related to the stretching vibrational bands of Mo-O and Mo-O-Mo.[14,15] The similarity of the IR spectra with those reported suggests the formation of KMO phase. Unlike Cu and Ni-doped $K_2Mo_4O_{13}$ compositions, no new bands were observed in KMO-Eu and KMO-Dy, probably due to the very low concentration of rare earth (Eu and Dy) ions.

Raman Spectroscopy

The Raman profiles of KMO and representative Ln (Eu/Dy) doped KMO were recorded to complement the results obtained from IR spectra. The Raman profiles are shown in Fig.-5B. All the compositions exhibit a strong Raman band at around 960 cm^{-1} along with low-intensity peaks.

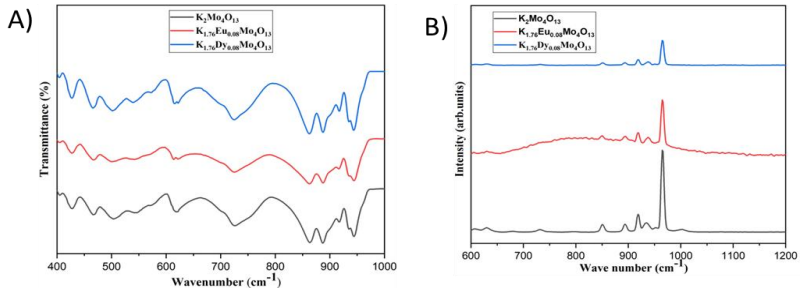

Fig.-5: A) Infrared Spectra of $K_2Mo_4O_{13}$, $K_{1.76}Eu_{0.08}Mo_4O_{13}$ and $K_{1.76}Dy_{0.08}Mo_4O_{13}$. B) Raman Profiles of $K_2Mo_4O_{13}$, $K_{1.76}Eu_{0.08}Mo_4O_{13}$ and $K_{1.76}Dy_{0.08}Mo_4O_{13}$

Photoluminescence Studies

Eu^{3+} Excitation Spectra

Trivalent europium is one of the rare earth ions with excellent persistent luminescent properties. The ground state of Eu^{3+} with electronic configuration $4f^6$ is $^7F_0$. The excitation spectra of all Eu-doped KMO samples were measured with in the 320-440 nm region by setting the emission wavelength at 615 nm. All

the excitation spectra show a strong band at 395 nm. The excitation spectrum of representative $K_{1.58}Eu_{0.14}MO_4O_{13}$ is depicted in Fig.-6a. The excitation spectrum is pigeonholed by a few peaks at 362, 380, 394 and 414 nm. The identification of the peaks was carried out by comparing the excitation spectrum with those of Eu^{3+} doped in oxide crystalline matrices. These peaks are due to 4*f*-4*f* electron transitions of the Eu^{3+} ion in the KMO lattice. The bands at 362 and 414 nm have the lowest intensity, while the peak at 395 nm has the highest intensity. The peak at 380 nm possesses medium intensity. The bands at 362, 380, 395 and 414 nm are due to $^7F_0 \rightarrow {}^5D_4$, $^7F_0 \rightarrow {}^5L_7$, $^7F_0 \rightarrow {}^5L_6$, and $^5F_0 \rightarrow {}^5D_3$ transitions, respectively.[16]

Eu^{3+} Emission Spectra

In general, the most intense band noticed in the excitation spectrum is used for recording the emission spectra of the samples. As mentioned earlier, the excitation spectra of all Eu doped KMO samples showed a strong band at 395 nm; it was fixed as the excitation wavelength region (550-725 nm) to record the emission spectra. The emission spectra of all Eu^{3+} doped KMO are provided in Fig.-6(b). All the Eu^{3+} doped $K_2MO_4O_{13}$ compositions exhibit a few bands at 591, 615, 650, and 694 nm. All these bands fall in the orange and red colours of the visible region. The bands at 591, 615, 650 and 694 nm arise due to the electron transitions $^5D_0 \rightarrow {}^7F_1$, $^5D_0 \rightarrow {}^7F_2$, $^5D_0 \rightarrow {}^7F_3$ and $^5D_0 \rightarrow {}^7F_4$, respectively. Although the excitation at 395 nm corresponds to the $^5L_6$ state, which is situated above the ^5D_J (J=1,2,3), the emission from these states to $^7F_0$ is absent due to non-radiative multiphonon relaxation to the $^5D_0$ level (Fig.-6c).[17] The emission band observed at a peak at 591 nm is related to the magnetic dipole transition, which follows the selection rule $\Delta J = 1$ and the peak at 615 nm is attributed to the electric dipole transition governed by the selection rule $\Delta J = 2$. A close observation of spectral profiles all the Eu doped compositions show that they are similar with respect to their peak positions, while the emission intensity varies with a change in dopant concentration. The intensity of emission bands increses progressively with increasing Eu^{3+} content and reaches a maximum at 14 mol%. Concentration quenching is not observed up to 14 mol% of Eu. It is noticed that the intensity and peak position of particular transitions of some rare earth ions are highly influenced by the environment present around the ion. These are termed as "hypersensitive" transitions and follow the selection rules, $|\Delta S = 0|$, $|\Delta L \leq 2|$ and $|\Delta J \leq 2|$.[18] In the case of the Eu^{3+} ion, the electrical dipole ($^5D_0 \rightarrow {}^7F_2$) transition is hypersensitive to the surrounding environment, whereas the magnetic dipole ($^5D_0 \rightarrow {}^7F_1$) transitions are relatively insensitive to the crystal field present around the lanthanide ion. Commonly, the PL intensity ratio of ED (electrical dipole) to MD (magnetic dipole) transitions is used to evaluate the inversion symmetry of Eu^{3+} ion in the host lattice. The dominance of ED transition ($^5D_0 \rightarrow {}^7F_2$) over MD ($^5D_0 \rightarrow {}^7F_1$) transition indictaes that guest ion (Eu^{3+}) occupies a site of non-inversion symmetry.[2]

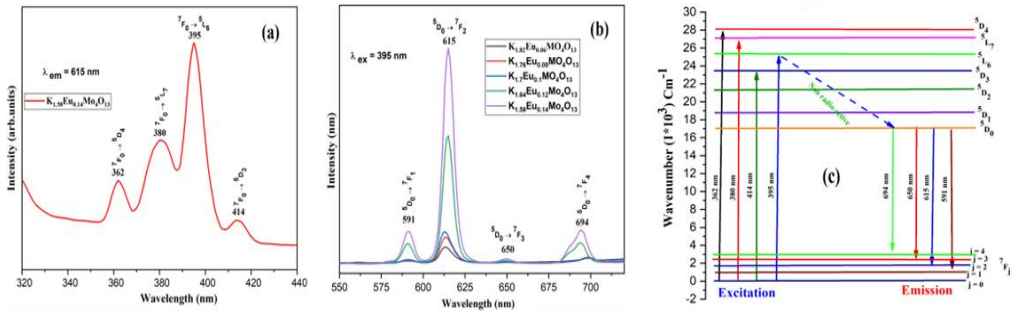

Fig.-6: Photoluminescence (a) Excitation Spectrum of $K_{1.58}Eu_{0.14}Mo_4O_{13}$, (b) Emission Spectra of $K_{1-3x}Eu_xMo_4O_{13}$, and (c) Energy Level Scheme of all the Observed Transitions of KMO-Eu

Dy^{3+} Excitation Spectra

The excitation profiles of all Dy^{3+} doped $K_2Mo_4O_{13}$ compositions were obtained while monitoring the emission wavelength set to 576 nm. The excitation spectrum of a representative 0.1 mol% of Dy^{3+} doped $K_2Mo_4O_{13}$ phosphor is shown in Fig.-7a. It is characterised by a few bands in the 300-500 nm region. The excitation spectrum consists of two regions: the first one in the 300-325 nm region comprises tailing (possibly due to a strong and broad band), which is due to the charge transfer (CT) band of $O^{2-} \rightarrow Mo^{6+}$,

while the second part is made up of sharp peaks in the 325-500 nm region. These sharp peaks are due to *4f – 4f* transitions of the Dy^{3+} ion. The peaks at 353, 387, 427, 453 and 470 nm belong to the electron transitions between $^6H_{15/2}$ to $^6P_{7/2}$, $^4I_{11/2}$, $^4I_{13/2}$, $^4I_{15/2}$ and $^4F_{9/2}$ states, respectively. Among these transitions, the intensity of the peak at 427 nm is high, and therefore it was chosen as excitation wavelength for emission measurements.

Dy^{3+} Emission Spectra

The ground state of Dy^{3+} with an electronic configuration of $4f^9$ is $^6H_{15/2}$. The emission spectra of Dy^{3+} in $K_2MO_4O_{13}$ host were obtained in the region of 550-650 nm by exciting at 427 nm (Fig.-7b). Two peaks are located at 576 and 638 nm, which are due to $^4F_{9/2}\rightarrow{}^6H_{13/2}$ and $^4F_{9/2}\rightarrow{}^6H_{11/2}$ transitions of the Dy^{3+} ion, respectively. In general, for the Dy^{3+} ion, three transitions in the visible region are expected. They are (a) $^4F_{9/2}\rightarrow{}^6H_{15/2}$ at 470-480 nm in the blue region, (b) $^4F_{9/2}\rightarrow{}^6H_{13/2}$ at 570-580 nm in the yellow region and (c) $^4F_{9/2}\rightarrow{}^6H_{11/2}$ at 630 - 680 nm in the orange region. Most of the crystalline and glassy matrices containing Dy^{3+} ion give the first two transitions (i.e. 470-480 and 570-580 nm peaks).[19] In the present investigation, however, the last two transitions at 576 nm and 638 nm are observed when excited at 427 nm. Emission spectra were also recorded by exciting at 353 nm (another strong band in the excitation spectrum). At this excitation wavelength, the same two emission bands (at 576 nm and 638 nm) were observed. One possible reason for the absence of 470-480 nm is cross-relaxation between $^4F_{9/2}$ and $^6H_{15/2}$ states. The intensity of these bands is found to increase with increase in Dy^{3+} ion concentration up to x = 0.06 mol%. Above this concentration limit, the decline in emission intensity was observed owing to the well-known phenomenon of concentration quenching.

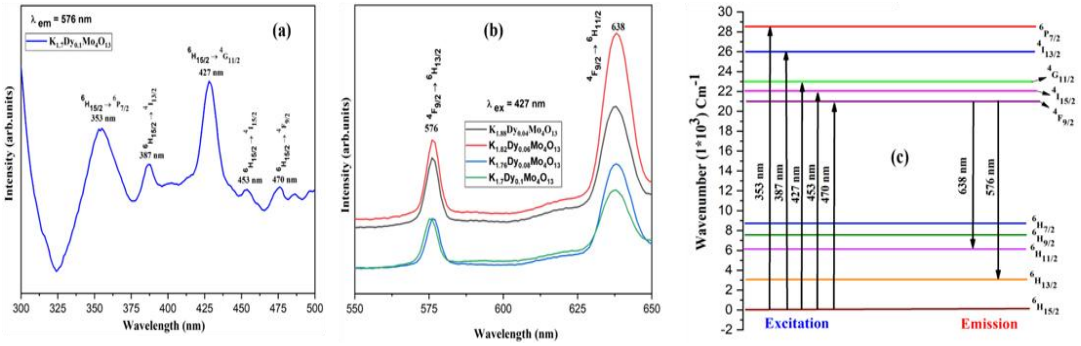

Fig.-7: Photoluminescence (a) Excitation Spectrum of $K_{1.7}Eu_{0.1}Mo_4O_{13}$, (b) Emission Spectra of $K_{1-3x}Dy_xMo_4O_{13}$, and (c) Energy Level Scheme of all the Observed Transitions of KMO-Dy

CONCLUSION

Pristine KMO and Eu (Dy) doped KMO were fruitfully prepared by solid-state and ion exchange methods, respectively. Both KMO and Eu (Dy) doped KMO were crystallised in a triclinic lattice. The formation of KCl in the reaction confirms the doping of Eu (Dy) into the KMO lattice. The EDS and Elemental mapping profiles also support the incorporation of Eu (Dy) ions into the structure of KMO. The IR and Raman profiles are similar to each other and consistent with reported data. The Eu^{3+} doped $K_2MO_4O_{13}$ compositions exhibit a few bands at 591, 615, 650, and 694 nm upon excitation at 395 nm corresponding to the $^5L_6$ state. These bands correspond to $^5D_0 \rightarrow {}^7F_1$, $^5D_0 \rightarrow {}^7F_2$, $^5D_0 \rightarrow {}^7F_3$ and $^5D_0 \rightarrow {}^7F_4$ respectiveley. The emission from the $^5L_6$ state was absent due to non-radiative multiphonon relaxation to the $^5D_0$ level. The concentration quenching of emission spectra was not observed up to 14 mol% of Eu doping. The intensity of the ED transition ($^5D_0 \rightarrow {}^7F_2$) is higher than that of the MD ($^5D_0 \rightarrow {}^7F_1$) transition, indicating that the guest ion (Eu^{3+}) is positioned at a site of non-inversion symmetry. Among all Dy^{3+} concentrations, 0.06 mol Dy^{3+} doped $K_2Mo_4O_{13}$ shows the highest emission intensity, and the intensity declines with increase in Dy^{3+} content, which leads to a concentration quenching mechanism in the phosphors. For the Dy^{3+} ion, the transition, $^4F_{9/2}\rightarrow{}^6H_{13/2}$, is highly sensitive to the surrounding host environment and it is predominantly an electric dipole (ED) character. In contrast, the other transition $^4F_{9/2}\rightarrow{}^6H_{11/2}$ arises mainly from a magnetic dipole (MD) process and it is relatively unaffected by changes in the host environment.

ACKNOWLEDGMENTS

The authors gratefully acknowledge Dr. B. R. Ambedkar University, Etcherla, Andhra Pradesh, for providing support and encouragement to carry out this work as part of the thesis research. The authors also thank the Research Centre, Government Degree College for Men, Srikakulam, for laboratory support. No financial support was received for this study.

CONFLICT OF INTERESTS

The authors declare that there is no conflict of interest.

AUTHOR CONTRIBUTIONS

The present work is related to *SDG-7: Affordable and Clean Energy*. All the authors contributed significantly to this manuscript, participated in reviewing/editing and approved the final draft for publication. The research profile of the authors can be verified from their ORCID ids, given below:

S. Dhilleswararao http://orchid.org/0009-0003-8812-084X
S. Ramakrishna https://orcid.org/0000-0002-4917-615X

Cite this article as: S. Dhilleswararao and S. Ramakrishna, *Rasayan J. Chem.*, 19(2), 831-838(2026), https://doi.org/10.317 88/RJC.2026.1929609.

REFERENCES

1. A. Setlur, E. V. Radkov, C. S. Henderson, J. H. Her, A. M. Srivastava, K. Nagaveni, M. S. Kishore, N. P. Kumar, D. Aesram, A. Deshpande, B. Kolodin, L.S. Grigorov and U. Happek, *Chemistry of Materials*, **22**, 4076(2010), https://doi.org/10.1021/cm100960g
2. J. Cho, J. H. Park and J. K. Kim, *Laser & Photonics Reviews*, **11**, 1600147(2017), https://doi.org/10.1002/lpor.201600147
3. M. Shang, C. Li and J. Lin, *Chemical Society Reviews*, **43**, 1372(2014), https://doi.org/10.1039/C3CS60314H
4. R. Boonsin, G. Chadeyron, J. P. Roblin, D. Boyer and R. Mahiou, *Journal of Materials Chemistry C*, **3**, 9580(2015), https://doi.org/10.1039/C5TC01516B
5. H. D. Nguyen, C. C. Lin, M. H. Fang and R. S. Liu, *Journal of Materials Chemistry C*, **2**, 10268(2014), https://doi.org/10.1039/C4TC02062F
6. H. S. Jang, H. Yang, S. W. Kim, J. Y. Han, S. G. Lee and D. Y. Jeon, *Advanced Materials*, **20**, 2696(2008), https://doi.org/10.1002/adma.200702846
7. R. J. Xie, N. Hirosaki, T. Suehiro, F. F. Xu and M. Mitomo, *Chemistry of Materials*, **18**, 5578(2006), https://doi.org/10.1021/cm061010n
8. F. Goutenoire, O. Isnard, R. Retoux and P. Lacorre, *Journal of Materials Chemistry*, **11**, 119(2001), https://doi.org/10.1039/B002962I
9. V. D. Sokolovskii, *Catalysis Reviews-Science and Engineering*, **32**, 1(1989), https://doi.org/10.1080/01614949009349939
10. E. Sani, A. Toncelli, M. Tonelli, D. A. Lis, E. V. Zharikov, K. A. Subbotin and V. A. Smirnov, *Journal of Applied Physics*, **97**, 123531(2005), https://doi.org/10.1063/1.1938276
11. A. M. Kaczmarek and R. Van Deun, *Chemical Society Reviews*, **42**, 8835(2013), https://doi.org/10.1039/C3CS60166H
12. B. M. Gatehouse and P. Leverett, *Journal of the Chemical Society A: Inorganic, Physical, Theoretical*, 2107(1971), https://doi.org/10.1039/J19710002107
13. K. Eda, K. Chin, N. Sotani and M. S. Whittingham, *Journal of Solid State Chemistry*, **177**, 916(2004), https://doi.org/10.1016/j.jssc.2003.09.029
14. M. Kassem, *Research on Chemical Intermediates*, **41**, 2891(2015), https://doi.org/10.1007/s11164-013-1397-4

15. M. Kassem, *Acta Metallurgica Sinica (English Letters)*, **27**, 180(2014), https://doi.org/10.1007/s40195-014-0030-x
16. Q. Wei and D. Chen, *Central European Journal of Physics,* **8**, 766(2010), https://doi.org/10.2478/s11534-009-0098-5
17. C. H. Kam and S. Buddhudu, *Physica B: Condensed Matter*, **344**, 182(2004), https://doi.org/10.1016/S0921-4526(03)00409-5
18. C. K. Jørgensen and B. R. Judd, *Molecular Physics*, **8**, 281(1964), https://doi.org/10.1080/00268976400100321
19. G. Lakshminarayana, J. Qiu, M. G. Brik and I. V. Kityk, *Journal of Physics: Condensed Matter*, **20**, 335106(2008), https://doi.org/10.1088/0953-8984/20/33/335106

[RJC-9609/2026]